# Ribosome profiling at isoform level reveals an evolutionary conserved impact of differential splicing on the proteome

Marina Reixachs-Solé[1], Jorge Ruiz-Orera[2], M Mar Alba[2,3], Eduardo Eyras[2,4,*],

[1]Pompeu Fabra University, E08003 Barcelona, Spain.
[2]IMIM - Hospital del Mar Medical Research Institute. E08003 Barcelona, Spain.
[3]Catalan Institution for Research and Advanced Studies. E08010 Barcelona, Spain
[4]The John Curtin School of Medical Research, Australian National University, Acton ACT 2601, Canberra, Australia

*correspondence to: eduardo.eyras@anu.edu.au

## Abstract

The differential production of transcript isoforms from gene loci is a key mechanism in multiple biological processes and pathologies. Although this has been exhaustively shown at RNA level, it remains elusive at protein level. Here, we describe a new pipeline ORQAS (ORF quantification pipeline for alternative splicing) for the translation quantification of individual transcript isoforms using ribosome-protected mRNA fragments (Ribosome profiling). We found evidence of translation for 40-50% of the expressed transcript isoforms in human and 50% in mouse, with 53% of the expressed genes having more than one translated isoform in human, and 33% in mouse. Differential analysis revealed that about 40% of the splicing changes measured at RNA level in human were concordant with changes in translation; and that 21.7% of changes measured at RNA level, and 17.8% at translation level, were conserved between human and mouse. Furthermore, orthologous cassette exons preserving the directionality of the change were found enriched in microexons in a comparison between glia and glioma in both, and were conserved between human and mouse.. In summary, we established a moderate but widespread impact of differential splicing in the translation of isoforms and found evidence of an impact on the translation of microexons as a consequence of differential splicing. ORQAS is available at https://github.com/comprna/orqas

## Introduction

The alternative processing of transcribed genomic loci through transcript initiation, splicing, and polyadenylation, determine the transcript repertoire of cells (Brown et al. 2014). Differential production of transcript isoforms, especially through the mechanism of alternative splicing, is crucial in multiple biological processes such as cell differentiation, acquisition of tissue-specific functions, and DNA repair (Fiszbein and Kornblihtt 2017; Baralle and Giudice 2017; Shkreta and Chabot 2015), as well as in multiple pathologies (Ward and Cooper 2010; Singh and Eyras 2017; Cummings et al. 2017). Although analysis of RNA sequencing (RNA-seq) data from multiple samples has indicated a large diversity of transcript molecules (Pertea et al. 2018), genes express mostly one single isoform in any given condition and this isoform may change across conditions (Gonzàlez-Porta et al. 2013; Sebestyén et al. 2015).

Computational and in-vitro studies have provided evidence that a change in relative isoform abundances can lead to the production of protein variants that impact the network of protein-protein interactions in different contexts (Buljan et al. 2012; Yang et al. 2016; Climente-González et al. 2017; Wojtowicz et al. 2007). In contrast, quantitative proteomics of naturally occurring proteins has identified much fewer protein variants than those predicted with RNA sequencing (Ezkurdia et al. 2015; Liu et al. 2017). Using state-of-the arts proteomics, it was recently shown that splicing changes at RNA level lead to changes in the sequence and abundance of proteins produced, although this was detectable for a limited number of transcripts (Liu et al. 2017). The difficulty in establishing a correspondence between transcript and protein variation may be due to limitations in current proteomics technologies, but also to the stability and translation regulation of transcripts (Maslon et al. 2014; Braun and Young 2014). Despite the large body of evidence describing its functional relevance (see e.g. (Baralle and Giudice 2017)), it is still debated whether differential splicing leads to fundamentally new proteins and how widespread protein variation might be (Tress et al. 2017a; Blencowe 2017; Tress et al. 2017b). Of particular interest are microexons, which can be as short as 3 nucleotides and carry out conserved neuronal-specific functions, and whose misregulation is linked to autism (Raj et al. 2014; Irimia et al. 2014; Quesnel-Vallieres et al. 2016). However, despite their involvement in protein-protein interactions (Ellis et al. 2012; Irimia et al. 2014), the detection of protein variation associated to differential microexon inclusion using unbiased proteomics is currently not possible.

Sequencing of ribosome-protected RNA fragments, i.e. ribosome profiling, provides information on the messengers being translated in a cell. In particular, it allows the identification of multiple translated open reading frames (ORFs) in the same gene and the discovery of novel translated

genes (Ingolia et al. 2009; Michel et al. 2012; Ruiz-Orera et al. 2014, 2015). However, ribosome profiling studies have been mainly oriented to gene-level analysis (Ingolia et al. 2009; Gonzalez et al. 2014; Ruiz-Orera et al. 2014). Recently, reads from ribosome profiling were mapped across the exon-exon junctions of alternative splicing events (Weatheritt et al. 2016), suggesting that alternative splicing products may be engaged by ribosomes and potentially translated to produce different protein isoforms. A potential limitation of that approach is that ribosomal profiling reads also contain signals from native, non-ribosomal RNA-protein complexes (Ji et al. 2016). As exon boundaries are profusely bound by RNA binding proteins and splicing factors (Witten and Ule 2011), the mapping of ribosome reads to these regions is not necessarily indicative of active translation. Additionally, ribosome activity is associated to signal periodicity and uniformity along open reading frames (Ji et al. 2015), which has not yet been tested in relation to transcript isoforms and alternative splicing. Thus, the extent to which alternative splicing, and in particular microexon inclusion, leads to the translation of alternative ORFs remains largely unknown.

In this article, we describe a new method, ORQAS (ORF quantification pipeline for alternative splicing), to quantify translation abundance at individual transcript level from ribosome profiling taking into account Ribosome signal periodicity and uniformity per isoform. We validated the translation quantification of isoforms using independent data from polysomal fractions and proteomics. We further found a concordance between differential splicing and differential translation, and obtained evidence for the differential translation of microexons that is conserved between human and mouse. ORQAS provides a powerful strategy to study the impacts of differential RNA processing in translation.

## Results

### Translation Abundance estimation at isoform level from Ribo-seq

We developed a new method, ORQAS (ORF quantification pipeline for alternative splicing), for the estimation of isoform-specific translation abundance (Fig. 1a) (Methods). ORQAS quantifies the abundance of open reading frames (ORFs) in RNA space from RNA sequencing (RNA-seq) in transcript per million (TPM) units, and assigns ribosome sequencing (Ribo-seq) reads to the same ORFs using RiboMap (Wang et al. 2016). After the assignment of Ribo-seq reads to isoform-specific ORFs, ORQAS calculates for each ORF two essential metrics to determine their potential translation: Uniformity, calculated as a proportion of the maximum entropy of the read distribution, and the 3nt periodicity along the ORF (Methods).

We analyzed with ORQAS Ribo-seq and matched RNA-seq data from human and mouse glia and glioma (Gonzalez et al. 2014), mouse hippocampus (Cho et al. 2015), and mouse embryonic stem cells (Sugiyama et al. 2017) (Supp. Table 1). To determine which values of uniformity and periodicity would be indicative of an isoform being translated, we selected as positive controls genes with a single annotated ORF and with evidence of protein expression in all 37 tissues recorded in the Human Protein Atlas (THPA) (Uhlén et al. 2015). We considered translated those ORFs within the 90% of the periodicity and uniformity distribution of these positive controls (Fig. 1b) (Supp. Fig. 1). This produced a total of 20709-20785 translated ORFs in human, and 13,019-17,515 in mouse (Supp. Table 2). Interestingly, a large fraction of the expressed protein-coding genes had multiple translated isoforms: 52,3%-54,9% of the genes in human (Figs. 1c and 1d) and 29.1%-35.9% in mouse (Supp. Figure 2).

Overall, the majority of translated isoforms correspond to either single-isoform genes or the isoform with the highest expression in a sample (main isoform) (Fig. 1d). However, from those genes with multiple isoforms expressed at the RNA level, 3,471-3,570 (52.6%-55.5%) of genes in human and 577-898 (27.6-34%) in mouse have an alternative isoform translated (Fig. 1d). From all translated isoforms, 47.3%-49.2% in human, and 28.3%-34.9% in mouse, correspond to alternative isoforms (secondary or other isoform, Fig. 1d). In genes with multiple isoforms, the main isoform showed the highest average Ribo-seq coverage compared to secondary isoforms, albeit not as high as for the single-ORF genes used as positive controls (Fig. 1e). As a quality control, we considered the proportion of isoforms with low or no RNA expression that fell inside our periodicity and uniformity cutoffs and found only 0.7-0.9% across the human samples and 0.1-1.5% in the mouse samples (Supp. Table 3).

**Ribosome profiling discriminates translation abundance at isoform level**

As an initial validation of the estimation of isoform-specific translation, we compared our predictions in human with immunohistochemistry data available from The Human Protein Atlas (Uhlén et al. 2015). We observed that genes with translated isoforms are more frequently validated at all levels of protein expression (Fig. 2a). Furthermore, the majority (96%) of genes with translated ORFs show some evidence of protein expression using a combination of protein features (Fig. 2b). To further validate our approach, we compared the translated isoforms predicted with ORQAS with the sequencing of RNA from polysomal fractions from the same human neuronal and embryonic stem cell samples (Blair et al. 2017). ORQAS predicted 27,552 translated isoforms in stem cells, and 25,034 in neurons (Supp. Fig. 3). We found that translated isoforms were enriched in polysomal fractions, whereas isoforms with RNA expression but not predicted to be translated with ORQAS were enriched in monosomal fractions (Fig. 2c), providing further support

to our predictions. This is also consistent with a small proportion of our predicted translated isoforms to be associated with NMD targets, which are generally associated with monosomes (Kim et al. 2017).

Cross-species conservation is a strong indicator of stable protein production (Ezkurdia et al. 2014). We thus decided to test the conservation of our translated isoforms in human and mouse, using glia and glioma samples available for both species. To this end, we used an optimization method to determine the human-mouse protein isoform pairs most likely to be functional orthologs (Methods) (Fig. 2d). From 15824 human-mouse 1-to-1 gene orthologs, we identified 18574 human-mouse protein isoform pairs representing potential functional orthologs. Moreover, 7,112 (64%) of the 1-to-1 gene orthologs had more than one orthologous isoform pair. We found that orthologous isoform pairs were significantly enriched in translated isoforms in both species (p-value < 2.2e-16 in all datasets) (Fig. 2e), providing further support for our predictions.

To perform an additional validation of our findings, we considered isoform-specific regions (Fig. 3a). We identified sequences that are unique to a specific isoform, since evidence mapped to these regions can be unequivocally assigned to the isoform. Additionally, we defined isoform-specific ORFs as sequences shared between two isoforms but with a different frame in each isoform, since protein evidence mapped to it can be confidently assigned to a specific ORF. Both region types in translated isoforms showed a higher density of reads per nucleotide compared with other isoforms (Fig. 3b) (Supp, Fig. 4a).

We further used peptides from Mass Spectrometry (MS) experiments (Vizcaíno et al. 2016) to match our predictions from Ribo-seq from the same tissue type (Methods). Overall we validated 86%-87% of translated single-ORF genes. Validation rate decreased with region length (Fig. 3c), as expected for MS experiments (Ezkurdia et al. 2014).

Additionally, since ORQAS quantification is performed for the entire ORF and not looking at specific regions within the ORF, we used the raw read data to validate the unique sequence regions. In total, 91-97% of unique sequence regions of length >200nt harbored uniquely mapping Ribo-seq reads (Fig. 3d) (Supp Fig. 4b), and 87-89% unique ORF regions of length > 200nt contained P-sites predicted from the mapped reads (Supp, Fig. 4c). Overall, we were able to validate 56-80% of the isoform-specific sequence regions tested and 48%-73% of the isoform-specific ORFs tested.

In summary, from all the protein-coding transcript isoforms considered from the annotation (84,024 in human and 48,928 in mouse), 58-59% in human and 63-65% in mouse showed RNA expression

> 0.1 TPM (Supp. Table 3). From these expressed isoforms, about 40% in human, 41-54% in mouse, were predicted to be translated by ORQAS, and 23-43% were validated using independent data, including conservation (Fig. 3e). Furthermore, about 10% of all the annotated alternative isoforms in human and mouse had evidence of translation and these represented 60% of all translated isoforms (Fig. 3f) (Supp Table 4). Our analyses thus indicate that, although they are a small fraction of all expressed transcripts, alternative transcript isoforms are often translated into protein.

**Conserved impact of differential splicing on translation**

Differential splicing is often assumed to lead to a measurable difference in protein production. However, at genome scale, this has only been shown for a limited number of cases (Liu et al. 2017). We addressed this question using our more sensitive approach based on Ribo-seq. We used SUPPA (Alamancos et al. 2015; Trincado et al. 2018) to obtain 37,676 alternative splicing events in human and 17,339 in mouse that covered protein coding regions (Methods). Using the same SUPPA engine to convert isoform abundances to event inclusion values (Alamancos et al. 2015; Trincado et al. 2018), we estimated the proportion of translation abundance, relative abundance (RA), explained by a particular alternative splicing event, using the isoform translation abundances (Fig. 4a). Accordingly, in analogy to a relative inclusion change (ΔPSI) in RNA space, we were able to measure the relative differences in ribosome space in relation to the inclusion or exclusion of particular alternative exons, or ΔRA.

Comparing the glia and glioma samples in human, we found 856 events with a significant change in RNA splicing (|ΔPSI|>0.1 and p-value<0.05), and 590 events with significant differential translation (|ΔRA|>0.1 and p-value<0.05), with a significant overlap of 363 events between them (Jaccard index, z-score=89.386 comparing to the Jaccard index distribution of the overlaps from subsample sets of the same size) (Fig. 4b). Similarly, in mouse we found an overlap of 179 events (Jaccard index z-score=65.326), between 471 events with a significant change in RNA splicing (|ΔPSI|>0.1 and p-value<0.05) and 240 with significant change in translation (|ΔRA|>0.1 and p-value<0.05) (Supp. Fig. 5a). Furthermore, considering the direction of change from all events in RNA and ribosome space, the concordance of the change was found to be significant for human (Pearson R=0.9904, p-value = 5.309e-312) and mouse (Pearson R=0.9937, p-value = 2.113e-170); and in particular for the events that were significant in both tests (Fig. 4c) (Supp. Fig. 5b).

We further observed a similar proportion of event types changing significantly in RNA and ribosome space, with an enrichment of exon skipping events in human (Fig. 4d) and mouse (Supp. Fig. 5c). In particular, microexons, defined to be of length ≤51nt (Li et al. 2015), were enriched in

the events changing between glia and glioma in both human (p-values 1.382e-12 for RNA-seq and 5.602e-10 for Ribo-seq) (Fig. 4e) and mouse (p-values 6.386e-16 for RNA-seq and 3.446e-06 for Ribo-seq) (Supp. Fig. 5d). We repeated the same analysis using data from human neuronal differentiation (Blair et al. 2017) and found that microexons were also enriched in the comparison between embryonic stem cells and neuronal cells in human for RNA splicing and translation changes (p-values 8.435e-06 for RNA-seq and 6.597e-05 for Ribo-seq) (Fig. 4f). Furthermore, using RNA sequencing from polysome fractions from the same stem cell and neuronal samples we were able to validate the change in inclusion patterns of microexons under the same conditions (Fig. 4g). These results provide evidence that differential splicing leads to a qualitative and quantitative change in the proteins produced from a gene locus. Our results are also consistent with a functional relevance of the inclusion of microexons in protein-coding transcripts in neuronal differentiation and their inclusion loss in brain-related disorders (Raj et al. 2014; Irimia et al. 2014).

To further test the relevance of our findings, we considered a set of 1,487 alternative exons conserved between human and mouse (Fig. 5a). A high proportion of them changed in the same direction between glia and glioma (66% in RNA-seq and 78% in Ribo-seq) (Fig. 5b). Moreover, we observed that microexons were enriched in these concordant changes in both species, with a general trend towards less inclusion in glioma (p-value 5.389e-05 in RNA-seq and 5.521e-4 for Ribo-seq) (Fig. 5c). Among the microexons with a differential pattern of splicing and translation, we identified one in the gene *GOPC*, which was linked before to glioblastoma (Charest et al. 2003), and one in the gene *CERS6* (Fig. 5d). To test further the potential relevance of the identified microexons with conserved differential pattern, we calculated their RNA splicing inclusion patterns across other normal and tumor brain samples. In particular, we analyzed samples from glioblastoma multiforme (GBM) from TCGA (Cancer Genome Atlas Research Network 2008), Neuroblastoma (NB) from TARGET (Pugh et al. 2013) (Fig 5e), and samples from cortex and hippocampus from GTEX (Carithers et al. 2015). Microexons with a conserved impact on translation recapitulate the pattern of decreased inclusion in GBM compared with the postmortem normal brain regions (Fig. 5e). Differentially translated microexons may explain tissue differentiation as well as tumor specific properties, as they differentiate tissues and tumor types (Supp. Fig. 5e), whereas conserved microexons appear to be more representative of the tissue differentiation (Supp. Fig. 5f).

## Discussion

We have described a new method, ORQAS, to obtain abundance estimates at isoform level in ribosome space (https://github.com/comprna/orqas). ORQAS allows the identification of multiple protein products from a gene and the study of differential translation associated to alternative

splicing and differential transcript usage between conditions. Our approach presents several novelties with respect to previous analyses (Blair et al. 2017; Weatheritt et al. 2016; Wang et al. 2016): i) we calculated the periodicity and uniformity for each isoform; ii) we validated our predictions using both sequence and ORF specific regions in isoforms, regardless whether these regions could be encoded into an standard alternative splicing event; and iii) we provided an isoform quantification in ribosome space that can be reused with other tools, like SUPPA. Additionally, ORQAS uses RNA-seq quantification to guide the isoform abundance estimation in ribosome space, unlike previous approaches that used directly Ribo-seq reads to quantify isoforms, which presents important limitations (Blair et al. 2017).

We estimated that in total about 40-50% of the protein coding isoforms with RNA expression showed some evidence of translation, and that around 20,700 proteins are produced in human and 13,000-17,500 in mouse in the tested conditions. Additionally, about 5,700-5,800 genes in human, 2,600-3,900 in mouse, produce more than one protein in those conditions. These estimates are far from what is generally predicted from RNA expression only (Pertea et al. 2018). This may be explained by the limited coverage of Ribo-seq reads, but may be also due to the fact that RNA-seq artificially amplifies fragments of unproductive RNAs leading to many false positives. Nonetheless, our data indicates that many more ORFs are translated in a given sample than what is detectable by current proteomics methods and the number of protein products are close to estimates using a combination of proteomics and sequence conservation (Ezkurdia et al. 2014). Importantly, we found that multiple ORFs are translated from the same gene and at different abundances across conditions.

Around 40% of the events detected with differential RNA splicing showed consistent measurable changes in Ribo-seq in the same direction, which supports the notion that changes in RNA processing of genes have a widespread impact in the translation of ORFs from a gene. In particular, we found that a pattern of decreased inclusion of microexons in glioma with respect to normal brain samples is recapitulated in translation, providing *in vivo* evidence that the splicing changes in microexons have an impact in protein production. Microexon inclusion is a hallmark of neuronal differentiation (Irimia et al. 2014; Raj et al. 2014; Trincado et al. 2018), and glia partly recapitulates the pattern of microexon inclusion found in neurons (Irimia et al. 2014). The decreased inclusion of microexons observed in glioma suggests a dedifferentiation pattern as has been described before for other tumors (Sebestyén et al. 2016), but could also be indicative of a difference in the content of neuronal cells in the samples compared. In either case, the evolutionary conservation of the change at RNA expression and protein production indicates a conserved functional program between the glia and glioma samples.

Our capacity to predict RNA splicing variations from RNA-seq data currently exceeds our power to evaluate the significance of those events regarding protein production with current proteomics technologies (Wang et al. 2018). Despite this limitation, mass spectrometry can show for a small number of cases that splicing changes impact the abundance of proteins produced by a gene (Liu et al. 2017). Our findings are in agreement with these results, and moreover overcome current limitations to determine genome-wide impacts of RNA processing changes on protein production. Furthermore, our analyses indicate that for the majority of genes producing multiple protein isoforms, these do not vary in more than 25% of the length of the most highly expressed isoform, suggesting that for most part, the functional impacts from alternative splicing are mediated by slight modifications in the protein sequences (Ellis et al. 2012), rather than through the production of essentially different proteins. In summary, ORQAS leverages ribosome profiling to provide a genome-wide coverage of genes and transcript isoforms and allow a more effective testing of the impacts of splicing in protein production, as well as the identification and validation of multiple proteins from the same gene locus.

## Methods

### Pre-processing of RNA-seq and Ribo-seq datasets

RNA-seq and Ribo-seq datasets were downloaded from Gene Expression Omnibus (GEO) for the following samples: normal glia and glioma from human and mouse (GSE51424) (Gonzalez et al. 2014), mouse hippocampus (GSE72064) (Cho et al. 2015), mouse embryonic stem cells (GSE89011) (Sugiyama et al. 2017), and three steps of forebrain neuronal differentiation in human (GSE100007) (Blair et al. 2017). Adapters in RNA-seq and Ribo-seq datasets were trimmed using cutadapt v.1.12 with additional quality filters (-hq = 30 -lq = 10) (Martin 2011). We further discarded reads that mapped to annotated rRNAs and tRNAs. Remaining reads in RNA-seq and Ribo-seq datasets were filtered by length (>= 26 nucleotides).

### Quantification of transcripts and open reading frames

We used the Ensembl annotation v85 for human (hg19) and mouse (mm10) removing pseudogenes, short isoforms (< 200 nt) and annotated isoforms with incomplete 5' or 3' regions. For the analysis of RNA-seq data we used Salmon v0.7.2 (Patro et al. 2017) to quantify transcript abundances in transcripts per million (TPM) units using the annotation of unique open reading frames (ORFs). To quantify coding sequences (CDS) at the isoform level with the Ribo-seq data we applied a modified version of Ribomap (Wang et al. 2016). As default, Ribomap uses the RNA-

seq reads aligned to the transcriptome sequences with STAR (Dobin et al. 2013). Instead, we provided a direct quantification of the ORFs with RNA-seq using Salmon, to be used as priors by RiboMap. We calculated the translation abundances of each ORF based on Ribo-seq in ORFs Per Million (OPM) units, analogously to the TPM units:

$$OPM_i = 10^6 \frac{n_i / l_i}{\sum_j n_j / l_j}$$

where $n_i$ is the estimated Ribo-seq counts in ORF $i$ and $l_i$ is the effective length of the same ORF.

**Identification of actively translated isoform coding sequences**

We identified actively translated ORFs by calculating two parameters read periodicity and read uniformity (Ji et al. 2015). The periodicity is based on the distribution of the reads in the annotated frame and the two alternative ones. In order to calculate the read periodicity, we previously computed the position of the P-site, corresponding to the tRNA binding-site in the ribosome complex. This was obtained by calculating the distance between annotated ATG start codons and the leftmost position covered by Ribo-Seq reads, for each read length, The uniformity was measured as the proportion of maximum entropy (PME) defined by the distribution of reads along the ORF:

$$H(X) = \sum_{i=1}^{n} \left(\frac{N_i}{N}\right) * log_2\left(\frac{N_i}{N}\right)$$

$$PME = \frac{H(X)}{\max(H)}$$

Where $N$ represents the total number of reads, $N_i$ is the number of reads in each region $i$ and *max(H)* is the entropy assuming that the reads are equally distributed across the ORF. The maximum value is 1, and indicates a completely even distribution of reads across codons. These values were obtained for each sample by pooling the replicates and we only considered ORFs with 10 or more assigned Ribo-seq reads, and with RNA-seq abundance TPM > 0.1.

**Polysomal fraction analysis**

We used RNA-seq from high polysomal, low polysomal and monosomal fractions from embryonic stem cells and neuronal cell culture in human (GSE100007) (Blair et al. 2017) to quantify isoforms with Salmon (Patro et al. 2017). Only ORFs from protein-coding isoforms were used for quantification. For each isoform we calculated the polysomal relative abundance as before (Maslon

et al. 2014) by dividing the abundance in high polysomal fraction in TPM units, by the sum of abundances in (high and low) polysomes and monosomes.

**Validation of isoform-specific regions**

We defined two different types of isoform-specific regions that were analysed differently. Isoform-specific sequences are regions with a unique nucleotide sequence among the isoforms of the same gene. Isoform-specific ORFs are defined as regions that will give rise to different amino-acid sequences within the proteins of the same gene, either because of the presence of isoform-specific sequences or frame-shifted common sequences (Fig. 3A). According to the annotation, we identified 34553 isoforms containing isoform-specific sequences in human and 29447 in mouse and 44298 isoforms containing isoform-specific ORFs in human and 34329 in mouse. For the validation of isoform-specific sequences we considered uniquely mapping Ribo-seq reads from the STAR output falling entirely inside these regions or in the junction of the specific sequence with the common region. Read densities inside those regions where calculated as the total number of uniquely mapping reads in the region divided by the length of the isoform-specific sequence. The validation of isoform-specific ORFs instead was performed using the profiles of counts in each base of the ORF considering the expected position of the P-site. For isoform-specific ORFs the read densities where established as total number of counts in the region divided by the length in nucleotides of the isoform-specific ORFs.

**Proteomics evidence in translated isoform coding sequences**

We mined the proteomics database PRIDE (Vizcaino et al. 2016) to search for peptide matches to ORFs. We only considered peptide datasets from mouse corresponding to tissues analyzed in this study: brain (PRD000010, PXD000349, PXD001786), hippocampus (PRD000363, PXD000311, PXD001135), and embryonic cell lines (PRD000522). This corresponded to a total of 328,200 peptides. We searched for peptide matches in translated ORFs and only kept peptides that had one perfect match to an ORF and did not have a match with 0, 1 or 2 amino acid mismatches to any other annotated ORF isoform from the same or different genes.

**Differential inclusion of events at RNA and translation level**

We used SUPPA (Alamancos et al. 2015; Trincado et al. 2018) to generate alternative splicing events defined from protein-coding transcripts and covering the annotated ORFs. The relative inclusion of an event was calculated with SUPPA in terms of the transcript abundances (in TPM units) calculated from RNA-seq and in terms of the ORF abundances (in OPM units) calculated

from Ribo-seq. The test for significant differential inclusion of the events was applied in the same way for both cases by testing the difference between the observed change between conditions and the observed change between replicates, as described before (Trincado et al. 2018).

**Calculation of orthologous isoforms**

We considered the set of 1-to-1 orthologous genes between human and mouse from Ensembl (v85) (Clamp et al. 2003). For each pair of orthologous genes we calculated all possible pairwise global alignments between the human and mouse proteins encoded by these genes using MUSCLE (Edgar 2004). For each alignment we defined a score as the fraction of amino acid matches over the total length of the global alignment, and kept only protein pairs with score >= 0.8. From all the remaining protein pairs in each orthologous gene pair, we selected the best human-mouse protein pairs using a symmetric version of the stable marriage algorithm (Eyras et al. 2004)

## Acknowledgements

We acknowledge funding from the Spanish Government and FEDER with grants BFU2015-65235-P, BIO2017-85364-R and MDM-2014-0370, and by Catalan Government (AGAUR) with grant SGR2017-1020. MR-S was funded by an FI grant from the Catalan Government with reference 2018FI_B1_00126.

## References

Alamancos GP, Pagés A, Trincado JL, Bellora N, Eyras E. 2015. Leveraging transcript quantification for fast computation of alternative splicing profiles. *RNA* **21**: 1521–1531.

Baralle FE, Giudice J. 2017. Alternative splicing as a regulator of development and tissue identity. *Nat Rev Mol Cell Biol* **18**: 437–451.

Blair JD, Hockemeyer D, Doudna JA, Bateup HS, Floor SN. 2017. Widespread Translational Remodeling during Human Neuronal Differentiation. *Cell Rep* **21**: 2005–2016.

Blencowe BJ. 2017. The Relationship between Alternative Splicing and Proteomic Complexity. *Trends Biochem Sci* **42**: 407–408.

Braun KA, Young ET. 2014. Coupling mRNA synthesis and decay. *Mol Cell Biol* **34**: 4078–87.

Brown JB, Boley N, Eisman R, May GE, Stoiber MH, Duff MO, Booth BW, Wen J, Park S, Suzuki AM, et al. 2014. Diversity and dynamics of the Drosophila transcriptome. *Nature* **512**: 393–9.

Buljan M, Chalancon G, Eustermann S, Wagner GP, Fuxreiter M, Bateman A, Babu MM. 2012. Tissue-Specific Splicing of Disordered Segments that Embed Binding Motifs Rewires Protein

Interaction Networks. *Mol Cell* **46**: 871–883.

Cancer Genome Atlas Research Network. 2008. Comprehensive genomic characterization defines human glioblastoma genes and core pathways. *Nature* **455**: 1061–8. http://www.ncbi.nlm.nih.gov/pubmed/18772890.

Carithers LJ, Ardlie K, Barcus M, Branton PA, Britton A, Buia SA, Compton CC, DeLuca DS, Peter-Demchok J, Gelfand ET, et al. 2015. A Novel Approach to High-Quality Postmortem Tissue Procurement: The GTEx Project. *Biopreserv Biobank* **13**: 311–9. http://www.ncbi.nlm.nih.gov/pubmed/26484571.

Charest A, Lane K, McMahon K, Park J, Preisinger E, Conroy H, Housman D. 2003. Fusion of FIG to the receptor tyrosine kinase ROS in a glioblastoma with an interstitial del(6)(q21q21). *Genes Chromosomes Cancer* **37**: 58–71.

Cho J, Yu N-K, Choi J-H, Sim S-E, Kang SJ, Kwak C, Lee S-W, Kim J, Choi D Il, Kim VN, et al. 2015. Multiple repressive mechanisms in the hippocampus during memory formation. *Science* **350**: 82–7.

Clamp M, Andrews D, Barker D, Bevan P, Cameron G, Chen Y, Clark L, Cox T, Cuff J, Curwen V, et al. 2003. Ensembl 2002: Accommodating comparative genomics. *Nucleic Acids Res* **31**.

Climente-González H, Porta-Pardo E, Godzik A, Eyras E. 2017. The Functional Impact of Alternative Splicing in Cancer. *Cell Rep* **20**: 2215–2226.

Cummings BB, Marshall JL, Tukiainen T, Lek M, Donkervoort S, Foley AR, Bolduc V, Waddell LB, Sandaradura SA, O'Grady GL, et al. 2017. Improving genetic diagnosis in Mendelian disease with transcriptome sequencing. *Sci Transl Med* **9**.

Dobin A, Davis CA, Schlesinger F, Drenkow J, Zaleski C, Jha S, Batut P, Chaisson M, Gingeras TR. 2013. STAR: Ultrafast universal RNA-seq aligner. *Bioinformatics* **29**: 15–21.

Edgar RC. 2004. MUSCLE: a multiple sequence alignment method with reduced time and space complexity. *BMC Bioinformatics* **5**: 113. http://www.ncbi.nlm.nih.gov/pubmed/15318951.

Ellis JD, Barrios-Rodiles M, Colak R, Irimia M, Kim T, Calarco J a, Wang X, Pan Q, O'Hanlon D, Kim PM, et al. 2012. Tissue-specific alternative splicing remodels protein-protein interaction networks. *Mol Cell* **46**: 884–92. http://www.ncbi.nlm.nih.gov/pubmed/22749401 (Accessed July 14, 2012).

Eyras E, Caccamo M, Curwen V, Clamp M. 2004. ESTGenes: Alternative splicing from ESTs in Ensembl. *Genome Res* **14**.

Ezkurdia I, Juan D, Rodriguez JM, Frankish A, Diekhans M, Harrow J, Vazquez J, Valencia A, Tress ML. 2014. Multiple evidence strands suggest that there may be as few as 19,000 human protein-coding genes. *Hum Mol Genet* **23**: 5866–78.

Ezkurdia I, Rodriguez JM, Carrillo-de Santa Pau E, Vázquez J, Valencia A, Tress ML. 2015. Most highly expressed protein-coding genes have a single dominant isoform. *J Proteome Res* **14**: 1880–7.

Fiszbein A, Kornblihtt AR. 2017. Alternative splicing switches: Important players in cell differentiation. *Bioessays* **39**.

Gonzàlez-Porta M, Frankish A, Rung J, Harrow J, Brazma A. 2013. Transcriptome analysis of human tissues and cell lines reveals one dominant transcript per gene. *Genome Biol* **14**: R70.

Gonzalez C, Sims JS, Hornstein N, Mela A, Garcia F, Lei L, Gass DA, Amendolara B, Bruce JN, Canoll P, et al. 2014. Ribosome profiling reveals a cell-type-specific translational landscape in brain tumors. *J Neurosci* **34**: 10924–36.

Ingolia NT, Ghaemmaghami S, Newman JRS, Weissman JS. 2009. Genome-wide analysis in vivo of translation with nucleotide resolution using ribosome profiling. *Science* **324**: 218–23.

Irimia M, Weatheritt RJ, Ellis JD, Parikshak NN, Gonatopoulos-Pournatzis T, Babor M, Quesnel-Vallières M, Tapial J, Raj B, O'Hanlon D, et al. 2014. A highly conserved program of neuronal microexons is misregulated in autistic brains. *Cell* **159**: 1511–23.

Ji Z, Song R, Huang H, Regev A, Struhl K. 2016. Transcriptome-scale RNase-footprinting of RNA-protein complexes. *Nat Biotechnol* **34**: 410–3.

Ji Z, Song R, Regev A, Struhl K. 2015. Many lncRNAs, 5'UTRs, and pseudogenes are translated and some are likely to express functional proteins. *Elife* **4**: e08890.

Kim WK, Yun S, Kwon Y, You KT, Shin N, Kim J, Kim H. 2017. mRNAs containing NMD-competent premature termination codons are stabilized and translated under UPF1 depletion. *Sci Rep* **7**: 15833.

Li YI, Sanchez-Pulido L, Haerty W, Ponting CP. 2015. RBFOX and PTBP1 proteins regulate the alternative splicing of micro-exons in human brain transcripts. *Genome Res* **25**: 1–13.

Liu Y, Gonzàlez-Porta M, Santos S, Brazma A, Marioni JC, Aebersold R, Venkitaraman AR, Wickramasinghe VO. 2017. Impact of Alternative Splicing on the Human Proteome. *Cell Rep* **20**: 1229–1241.

Martin M. 2011. Cutadapt removes adapter sequences from high-throughput sequencing reads. *EMBnet.journal* **17**: 10.

Maslon MM, Heras SR, Bellora N, Eyras E, Cáceres JF. 2014. The translational landscape of the splicing factor SRSF1 and its role in mitosis. *Elife* **2014**.

Michel AM, Choudhury KR, Firth AE, Ingolia NT, Atkins JF, Baranov P V. 2012. Observation of dually decoded regions of the human genome using ribosome profiling data. *Genome Res* **22**: 2219–29. http://www.ncbi.nlm.nih.gov/pubmed/22593554.

Patro R, Duggal G, Love MI, Irizarry RA, Kingsford C. 2017. Salmon provides fast and bias-aware quantification of transcript expression. *Nat Methods*.

Pertea M, Shumate A, Pertea G, Varabyou A, Breitwieser FP, Chang Y-C, Madugundu AK, Pandey A, Salzberg SL. 2018. CHESS: a new human gene catalog curated from thousands of large-scale RNA sequencing experiments reveals extensive transcriptional noise. *Genome Biol* **19**: 208. http://www.ncbi.nlm.nih.gov/pubmed/30486838.

Pugh TJ, Morozova O, Attiyeh EF, Asgharzadeh S, Wei JS, Auclair D, Carter SL, Cibulskis K, Hanna M, Kiezun A, et al. 2013. The genetic landscape of high-risk neuroblastoma. *Nat Genet* **45**: 279–84. http://www.ncbi.nlm.nih.gov/pubmed/23334666.

Quesnel-Vallieres M, Dargaei Z, Irimia M, Woodin MA, Blencowe BJ, Cordes SP. 2016. Misregulation of an Activity-Dependent Splicing Network as a Common Mechanism Underlying Article Misregulation of an Activity-Dependent Splicing Network as a Common Mechanism Underlying Autism Spectrum Disorders. *Mol Cell* 1023–1034.

Raj B, Irimia M, Braunschweig U, Sterne-Weiler T, O'Hanlon D, Lin Z-Y, Chen GI, Easton LE, Ule J, Gingras A-C, et al. 2014. A global regulatory mechanism for activating an exon network required for neurogenesis. *Mol Cell* **56**.

Ruiz-Orera J, Hernandez-Rodriguez J, Chiva C, Sabidó E, Kondova I, Bontrop R, Marqués-Bonet T, Albà MM. 2015. Origins of De Novo Genes in Human and Chimpanzee. *PLoS Genet* **11**: e1005721.

Ruiz-Orera J, Messeguer X, Subirana JA, Alba MM. 2014. Long non-coding RNAs as a source of new peptides. *Elife* **3**: e03523.

Sebestyén E, Singh B, Miñana B, Pagès A, Mateo F, Pujana MA, Valcárcel J, Eyras E. 2016. Large-scale analysis of genome and transcriptome alterations in multiple tumors unveils novel cancer-relevant splicing networks. *Genome Res* **26**.

Sebestyén E, Zawisza M, Eyras E. 2015. Detection of recurrent alternative splicing switches in tumor samples reveals novel signatures of cancer. *Nucleic Acids Res* **43**.

Shkreta L, Chabot B. 2015. The RNA Splicing Response to DNA Damage. *Biomolecules* **5**: 2935–77. http://www.ncbi.nlm.nih.gov/pubmed/26529031.

Singh B, Eyras E. 2017. The role of alternative splicing in cancer. *Transcription* **8**.

Sugiyama H, Takahashi K, Yamamoto T, Iwasaki M, Narita M, Nakamura M, Rand TA, Nakagawa M, Watanabe A, Yamanaka S. 2017. Nat1 promotes translation of specific proteins that induce differentiation of mouse embryonic stem cells. *Proc Natl Acad Sci U S A* **114**: 340–345.

Tress ML, Abascal F, Valencia A. 2017a. Alternative Splicing May Not Be the Key to Proteome Complexity. *Trends Biochem Sci* **42**: 98–110.

Tress ML, Abascal F, Valencia A. 2017b. Most Alternative Isoforms Are Not Functionally Important. *Trends Biochem Sci* **42**: 408–410.

Trincado JL, Entizne JC, Hysenaj G, Singh B, Skalic M, Elliott DJ, Eyras E. 2018. SUPPA2: Fast, accurate, and uncertainty-aware differential splicing analysis across multiple conditions. *Genome Biol* **19**.

Uhlén M, Fagerberg L, Hallström BM, Lindskog C, Oksvold P, Mardinoglu A, Sivertsson Å, Kampf C, Sjöstedt E, Asplund A, et al. 2015. Tissue-based map of the human proteome. *Science* **347**: 1260419–1260419.

Vizcaíno JA, Csordas A, Del-Toro N, Dianes JA, Griss J, Lavidas I, Mayer G, Perez-Riverol Y, Reisinger F, Ternent T, et al. 2016. 2016 update of the PRIDE database and its related tools. *Nucleic Acids Res* **44**: 11033.

Wang H, McManus J, Kingsford C. 2016. Isoform-level ribosome occupancy estimation guided by transcript abundance with Ribomap. *Bioinformatics* **32**: 1880–2.

Wang X, Codreanu SG, Wen B, Li K, Chambers MC, Liebler DC, Zhang B. 2018. Detection of Proteome Diversity Resulted from Alternative Splicing is Limited by Trypsin Cleavage Specificity. *Mol Cell Proteomics* **17**: 422–430. http://www.ncbi.nlm.nih.gov/pubmed/29222161.

Ward AJ, Cooper TA. 2010. The pathobiology of splicing. *J Pathol* **220**: 152–163.

Weatheritt RJ, Sterne-Weiler T, Blencowe BJ. 2016. The ribosome-engaged landscape of alternative splicing. *Nat Struct Mol Biol* **23**: 1117–1123.

Witten JT, Ule J. 2011. Understanding splicing regulation through RNA splicing maps. *Trends Genet* **27**: 89–97.

Wojtowicz WM, Wu W, Andre I, Qian B, Baker D, Zipursky SL. 2007. A vast repertoire of Dscam binding specificities arises from modular interactions of variable Ig domains. *Cell* **130**: 1134–45.

Yang X, Coulombe-Huntington J, Kang S, Sheynkman GM, Hao T, Richardson A, Sun S, Yang F, Shen YA, Murray RR, et al. 2016. Widespread Expansion of Protein Interaction Capabilities by Alternative Splicing. *Cell* **164**: 805–17.

## Figures

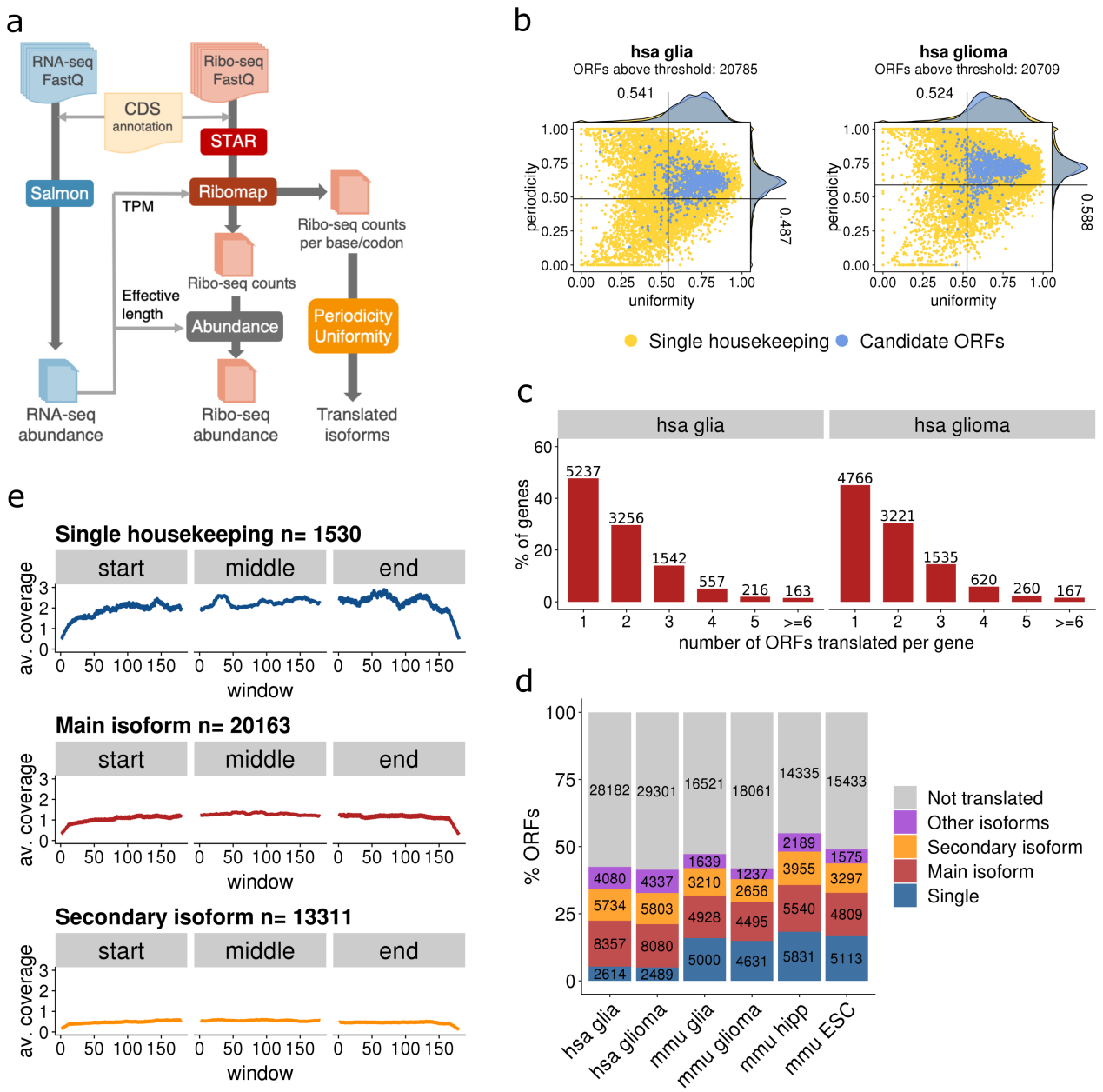


**Figure 1. Estimation of translated isoforms. (a)** The ORF quantification pipeline for alternative splicing (ORQAS) quantifies transcript abundances (ATXT) in transcripts per million (TPM) units from RNA-seq with Salmon (Patro et al. 2017) and in ORFs per million (OPM) units with Ribomap (Wang et al. 2016). Coverage and periodicity are calculated for every ORFs with TPM > 0.1, and candidate translated isoforms are estimated by comparing to a set of single-ORF house keeping genes with protein expression evidence across 37 tissues. **(b)** Uniformity (x axis) versus periodicity (y axis) for all tested ORFs with RNA expression TPM > 0.1 and at least 10 Ribo-seq reads assigned (in yellow). Uniformity is measured as the percentage of maximum entropy and periodicity is measured in the first annotated frame. Single-ORF house keeping genes are

indicated in blue. We show the data for human glia and glioma. Other samples are shown in Supp. Fig. 1. **(c)** Distribution of the number of different ORFs translated per gene in the human glia and glioma samples. Other samples are shown in Supp. Fig 2. **(d)** Number of ORFs predicted to be translated per sample, separated according to whether the ORF is encoded by: a single-ORF gene (Single), the most abundant isoform according to RNA-seq abundance in a gene with multiple isoforms (Main isoform), the second most abundant isoform (Secondary isoform), or by any of the remaining isoforms in the abundance ranking (Other isoforms). Tested ORFs that are not predicted to be translated are depicted in gray (Not-translated). **(e)** Average density of Ribo-seq reads along ORFs in housekeeping singleton genes, in ORFs from the most abundant isoform according to RNA-seq abundance in a gene with multiple isoforms, and in the second most abundant isoform.

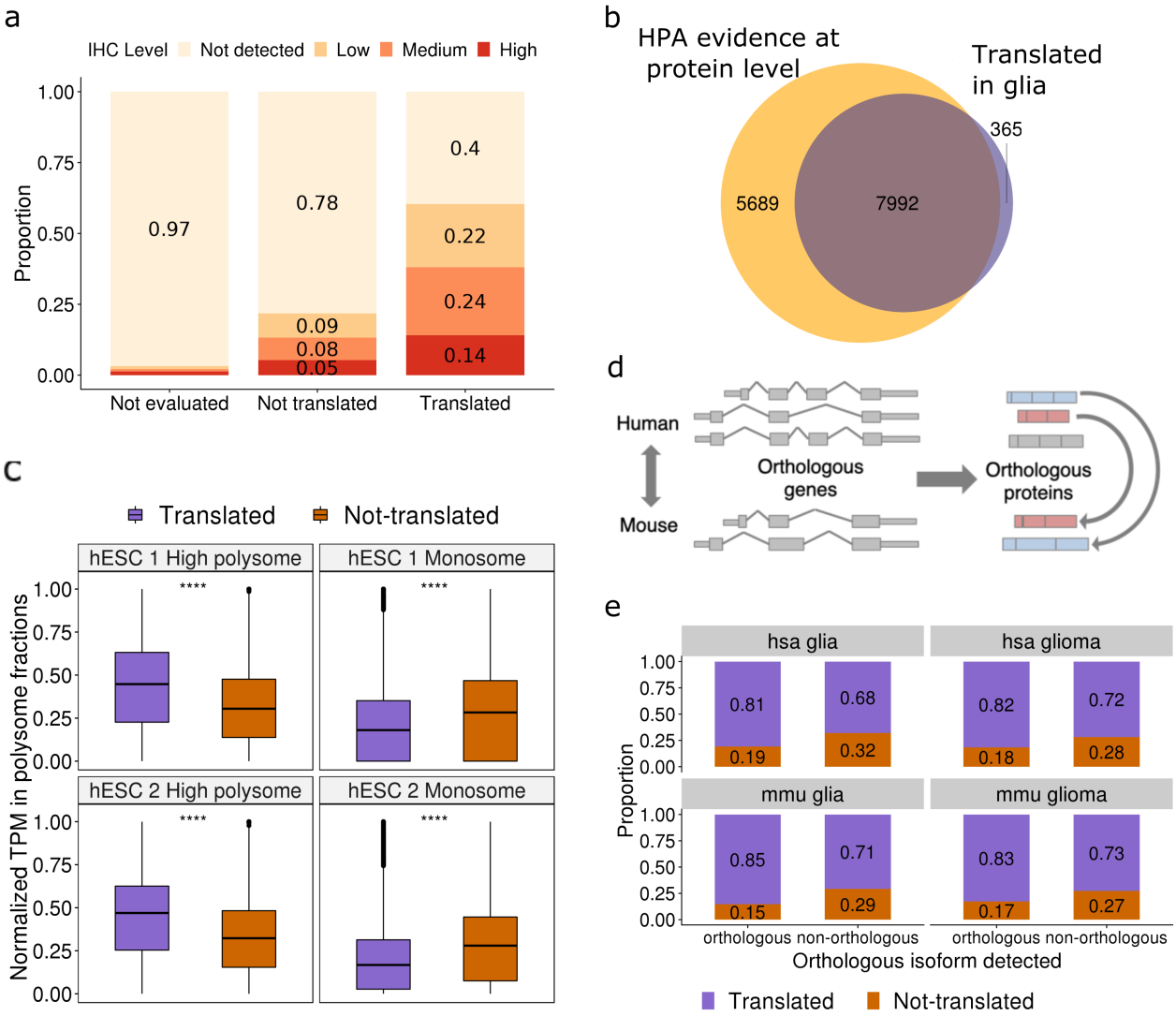


**Figure 2. Validation of predictions. (a)** For the candidate translated isoforms (translated), the cases that did not pass the threshold of uniformity and periodicity (not-translated), and those without enough read data to be tested (not evaluated), the plot shows the proportion of cases in which the corresponding gene has evidence from immunohistochemistry, separated as high, low, and medium expression, from the Human Protein Atlas (Uhlén et al. 2015). We also indicate the cases not detected in the immunohistochemistry experiments (not-detected). The comparison was made for the human glia Ribo-seq. Singletons (single-ORF genes) were not included. **(b)** The plot shows the number of genes with predicted translated ORFs that have evidence of protein expression in the Human Protein Atlas from a combination of features: Mass Spectrometry, Immunohistochemistry and Uniprot. Translation predictions correspond to human glia Ribo-seq. Singletons were not included. **(c)** We show the distribution of the relative abundance in high polysome (left panels) and monosome (right panels) fractions for translated isoforms and for isoforms with RNA expression (TPM>0.1) but predicted as not translated. The plot shows the

results for the two replicates for monosome (replicate 1 p-value = 3.61e-82 and replicate 2 p-value = 1.60e-152) and high polysome fractions for embryonic stem cells (replicate 1 p-value = 1.09e-230 and replicate 2 p-value = 2.41e-253). The results for neuronal cells are given in Supp. Fig. 3. **(d)** Cross-species conservation of protein isoforms. Protein isoforms from a 1-to-1 orthologous gene pair are compared and candidate orthologous pairs are assigned using an optimization approach (Methods). **(e)** For the set of ORFs encoding a human-mouse orthologous protein pair (orthologous) and for those encoding proteins without an orthologous pair in mouse (non-orthologous) we plot the percentage that are predicted to be translated (translated) and the ones with RNA expression (TPM>0.1) but predicted as not translated (not-translated). We show here the results for human glia (p-value = 1.41e-140 Fisher test) and glioma (p-value = 3.63e-85), and for mouse glia (p-value = 1.143e-130) and glioma (p-value = 7.462e-53), Other mouse samples are shown in Supp. Fig. 3.

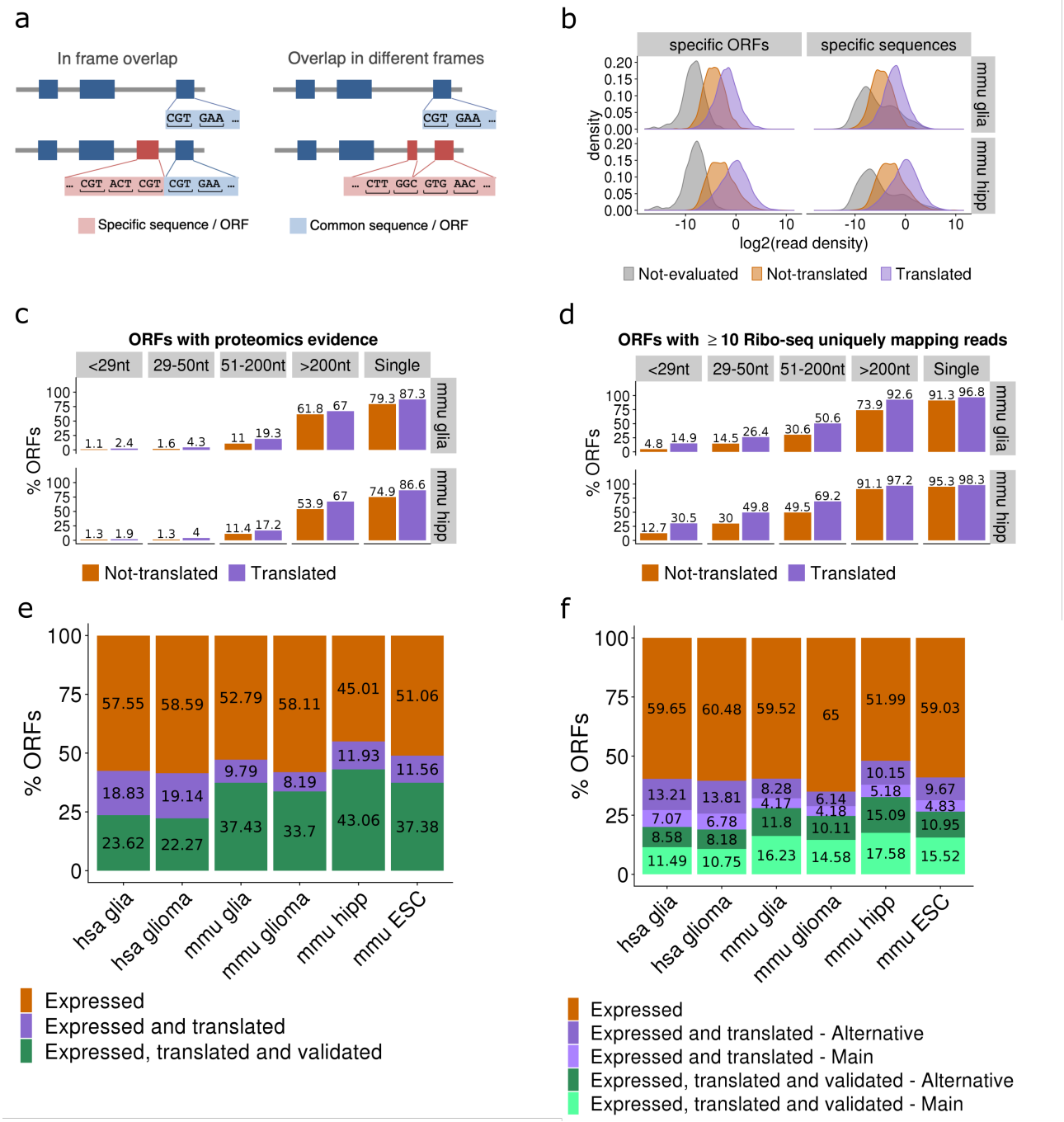


**Figure 3. Validation with Isoform-specific regions. (a)** Isoform-specific sequence regions (left panel) defined as the parts of an isoform ORF that are not present in any other isoform from the same gene (left panel). Isoform-specific ORFs (right panel) are defined AS a region shared between two isoforms, but with a different frame in each isoform. **(b)** For the mouse samples of glia (mmu glia) and hippocampus (mmu hipp) we show the density of Ribo-seq reads per nucleotide over the isoform-specific regions. The left panels show the counts per nucleotide based on the estimated P-site positions over region length in $\log_2$ scale for isoform-specific ORFs. The right panels show the uniquely mapping read-count over region length in $\log_2$ scale for isoform-specific sequences. Distributions are given for predicted translated isoforms, for isoforms that did

not pass the threshold of uniformity and periodicity (not translated), and for the isoforms with low expression (TPM<0.1) (not evaluated). Other samples are shown in Supp Fig. 4. **(c)** Validation with mass spectrometry peptides. For the mouse samples of glia (mmu glia) and hippocampus (mmu hipp), the plot shows the percentage of ORF-specific regions with 1 or more peptides, separated according to region length. We show these results for both types of regions: isoform-specific ORFs sequences and isoform-specific ORFs. Other samples are shown in Supp Fig. 4. **(d)** For the mouse samples of glia (mmu glia) and hippocampus (mmu hipp) the plot shows the percentage of regions with at least 10 uniquely mapping Ribo-seq reads in isoform-specific sequences over the total number of isoforms with an isoform-specific sequence defined according to the length of the region. Other samples are shown in Supp Fig. 4. **(e)** Proportion of isoforms expressed predicted to be translated and that have been validated using one or more sources of evidence: conservation, uniquely mapped Ribo-seq reads in specific sequences, counts per base in specific ORFs and peptides. For each sample, and for all ORFs with sufficient RNA-seq expression (TPM > 0.1), we show the proportion predicted to be translated from Ribo-seq reads and the proportion that were validated. The proportions are colored to indicate the fraction that is not included in the more restricted set: expressed > translated > validated. **(f)** For each sample, and for all ORFs with sufficient RNA-seq expression (TPM > 0.1), we show the proportion of main isoforms and alternative isoforms predicted to be translated from Ribo-seq reads and the proportion that were validated. These plots do not include the genes with a single protein-coding isoform.

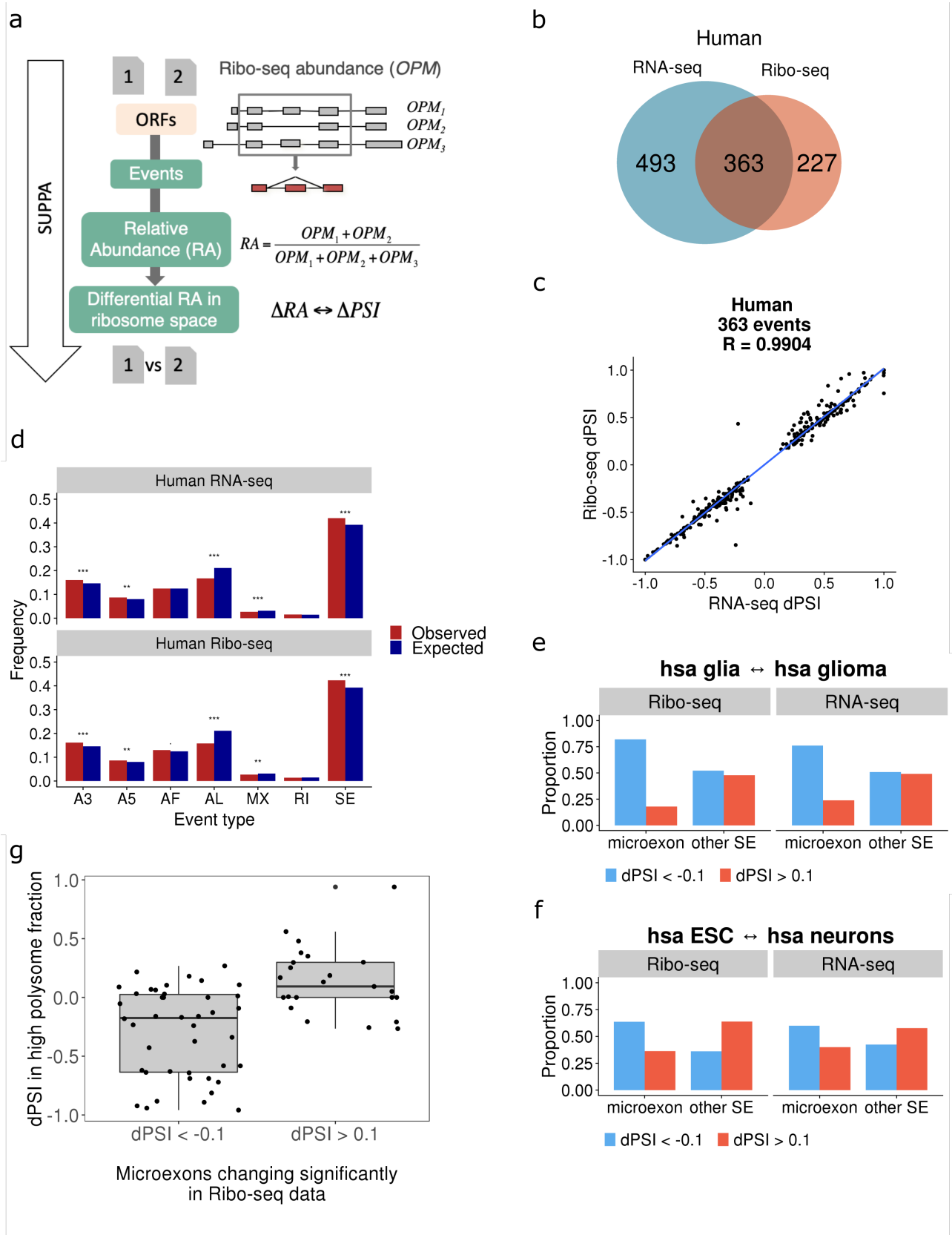


**Figure 4. Differential translation linked to differential splicing. (a)** Description of how SUPPA was used to calculate the differential inclusion of events in ribosome space. The abundance of open reading frames (ORFs) is calculated in ORFs per million (OPM) units. OPMs are transferred to events using SUPPA definition of events, using only exon-intron structures overlapping ORFs.

For each event a relative abundance (RA) is obtained, analogous to a PSI. **(b)** Overlap of events changing significantly (dPSI > 0.1 and p-value < 0.05) with RNA-seq and with Ribo-seq for human. **(c)** Correlation of changes in splicing and translation in events in human. **(d)** We show the proportions of events calculated in RNA space (upper panel) or in ribosome space (lower panel). In red we show the proportion of alternative splicing events calculated with SUPPA from the annotated coding regions in transcripts in human, whereas in blue we show the events that show a significant change using RNA-seq from mouse glia and glioma. Even types are: alternative 3'ss (A3) and 5'ss (A5), alternative first (AF) and last (AL) exon, mutually exclusive (MX) exon, retained introns (RI) and skipping exon (SE). There is significant enrichment for SE events for RNA (Fisher's test p-value = 3.90e-06) and Ribo-seq (p-value = 7.46e-07), for A3 events for RNA (p-value = 1.02e-05) and Ribo-seq (6.22e-06), for A5 events for RNA (4.55e-03) and Ribo-seq (8.73e-03); and significant depletion for AL events for RNA (1.73e-32) and Ribo-seq (2.43e-43) and for MX events for RNA (6.06e-04) and Ribo-seq (1.83e-03). These proportions for mouse are shown in Supp. Fig. 4. **(e)** Enrichment of microexons with an impact in RNA splicing and ORF translation in human from the comparison of glia and glioma samples. In the figure, dPSI is used to indicate the difference in relative abundance in both RNA and Ribosome spaces. **(f)** Enrichment of microexons with an impact in RNA splicing and ORF translation in human from the comparison of Embrionic Stem Cells (ESC) and neuronal samples. As before, dPSI indicates the difference in relative abundance in both RNA and Ribosome spaces. **(g)** Difference in high polysome fraction, measured as dPSI, between neuronal samples and ESCs (y axis) for microexons with a significant change in Ribosome space. As before, dPSI indicates the difference in relative abundance in Ribosome space.

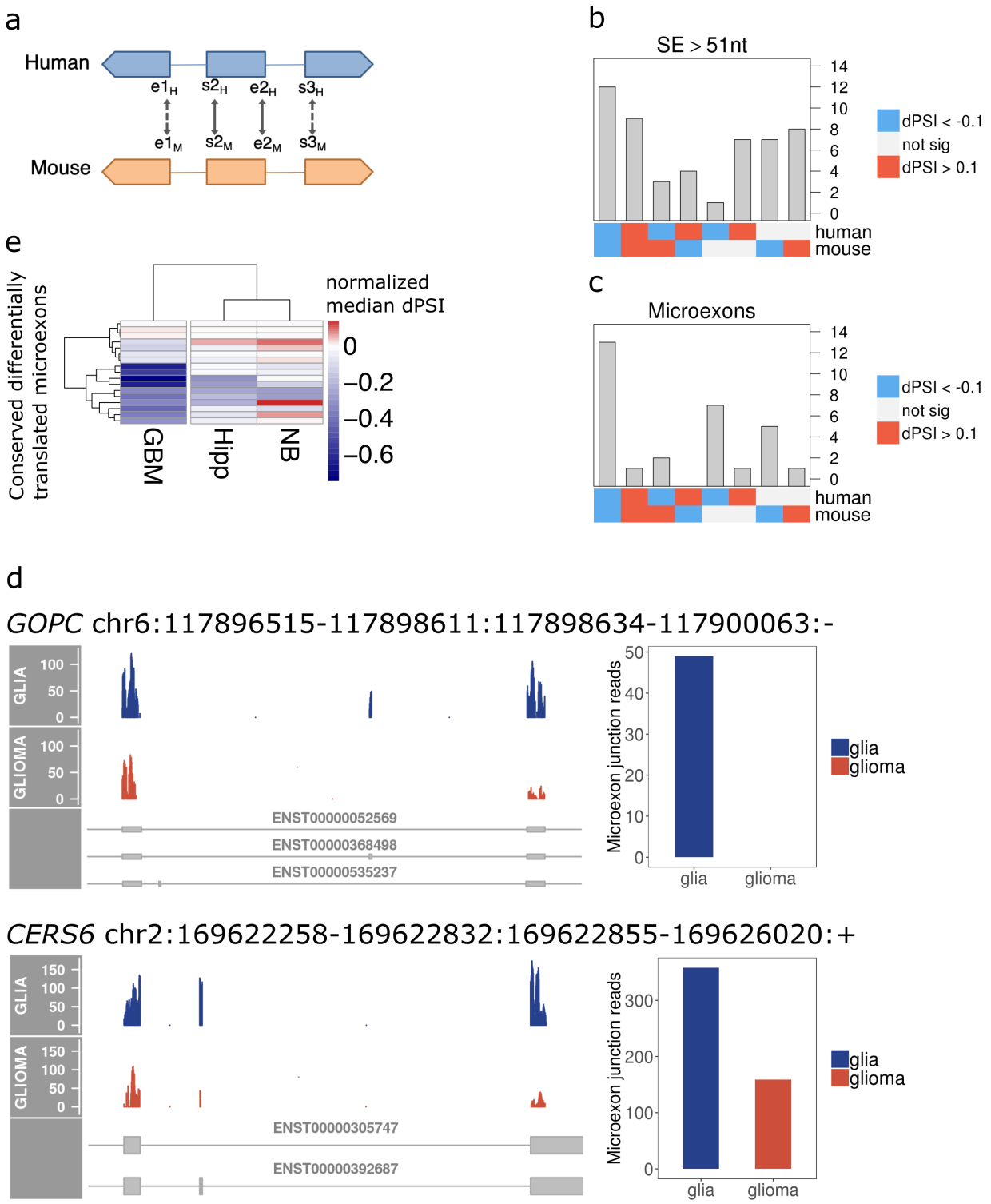


**Figure 5. A conserved program of differential RNA usage and translation. (a)** Conserved alternative splicing events were obtained by mapping with LiftOver the coordinates of the alternative exon (s2, e2), and the internal coordinates of the flanking exons (e1, s3). We considered those alternative exons as conserved if at least (s2, e2) were conserved. **(b)** Directionality of the changes in conserved alternative exons longer than 51nt in Ribosome space.

As before, dPSI indicates here the difference in relative abundance in both RNA and Ribosome spaces. **(c)** Directionality of the changes in evolutionary conserved alternative microexons (≤51nt) in Ribosome space. As before, dPSI indicates here the difference in relative abundance in both RNA and Ribosome spaces. **(d)** Examples of microexons that change significantly in RNA and ribosome space between glia and glioma. For the genes *GOPC* and *CERS6* we show Ribo-seq reads mapping to the microexon region and its flanking exons (left panels) and the number of Ribo-seq reads crossing the microexon junctions (right panels) in both glia (in blue) and glioma (in orange). **(e)** Patterns of inclusion of conserved differentially translated microexons in normal hippocampus (Hipp) samples from GTEX, gliblastoma multiforme (GBM) from TCGA, and neuroblastoma (NB) from TARGET. The heatmap shows the difference of the median PSI with respect to normal brain cortex tissue from GTEX.

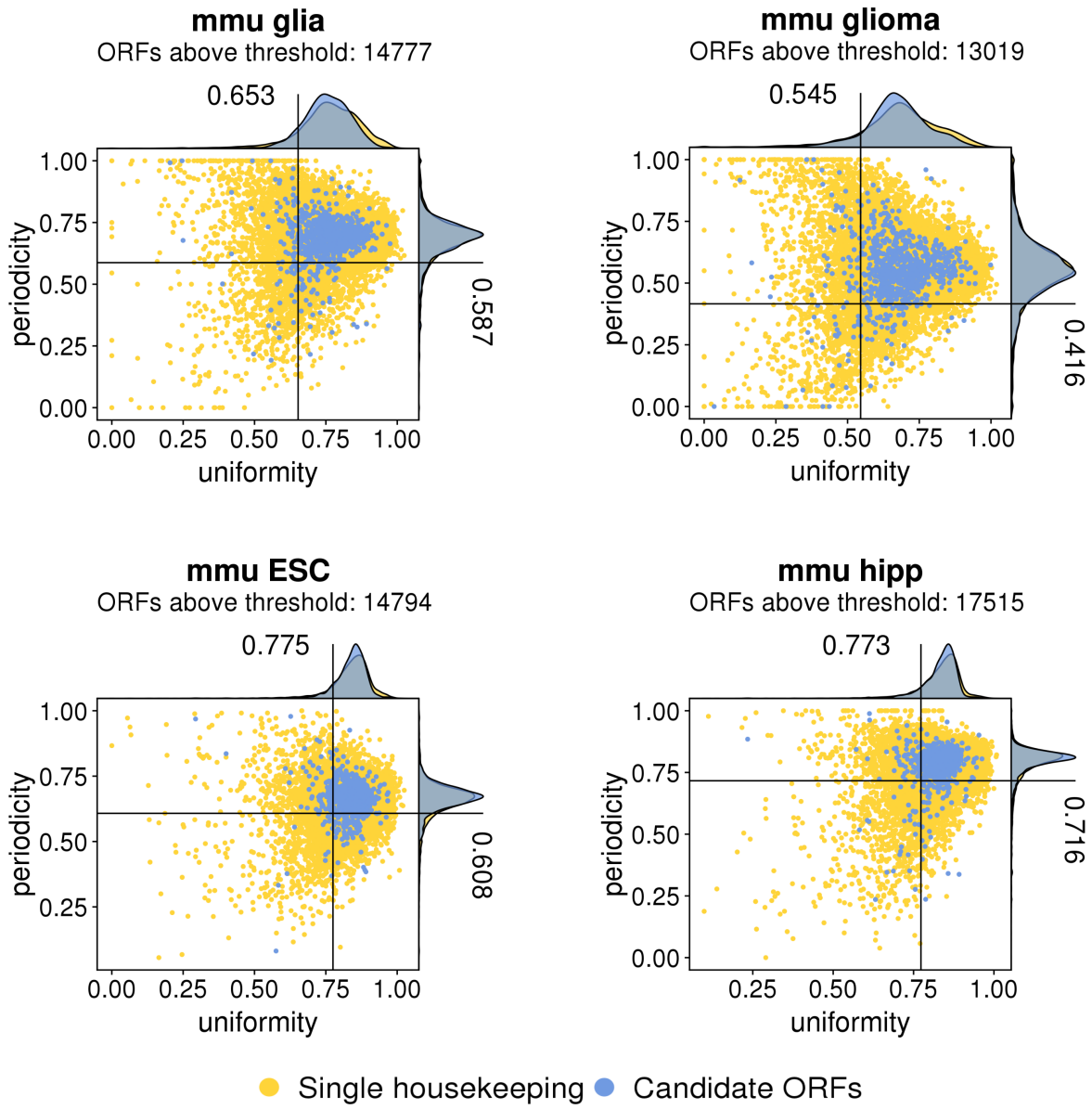


**Supplementary Figure 1.** Uniformity (x axis) versus periodicity (y axis) for the ORFs with with RNA expression TPM > 0.1 and at least 10 Ribo-seq reads assigned. In blue we indicate ORFs from genes defined as housekeeping singletons, and in yellow the rest of ORFs considered. Uniformity is measured as the percentage of maximum entropy and periodicity is measured in the first annotated frame. We show the data for mouse samples of glia (mmu glia), glioma (mmu glioma), Embrionic Stem Cells (mmu ESC) and hippocampus (mmu hipp).

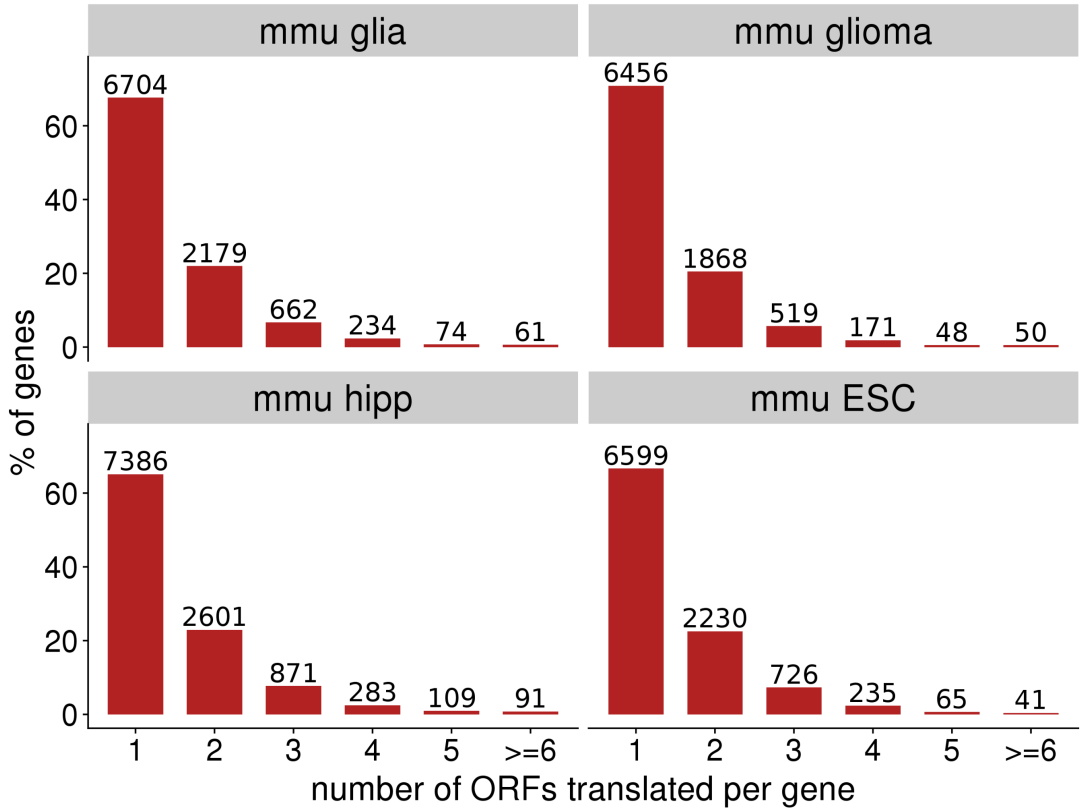


**Supplementary Figure 2.** Distribution of the number of different ORFs translated per gene in the mouse samples of glia (mmu glia), glioma (mmu glioma), hippocampus (mmu hipp) and Embrionic Stem Cells (mmu ESC).

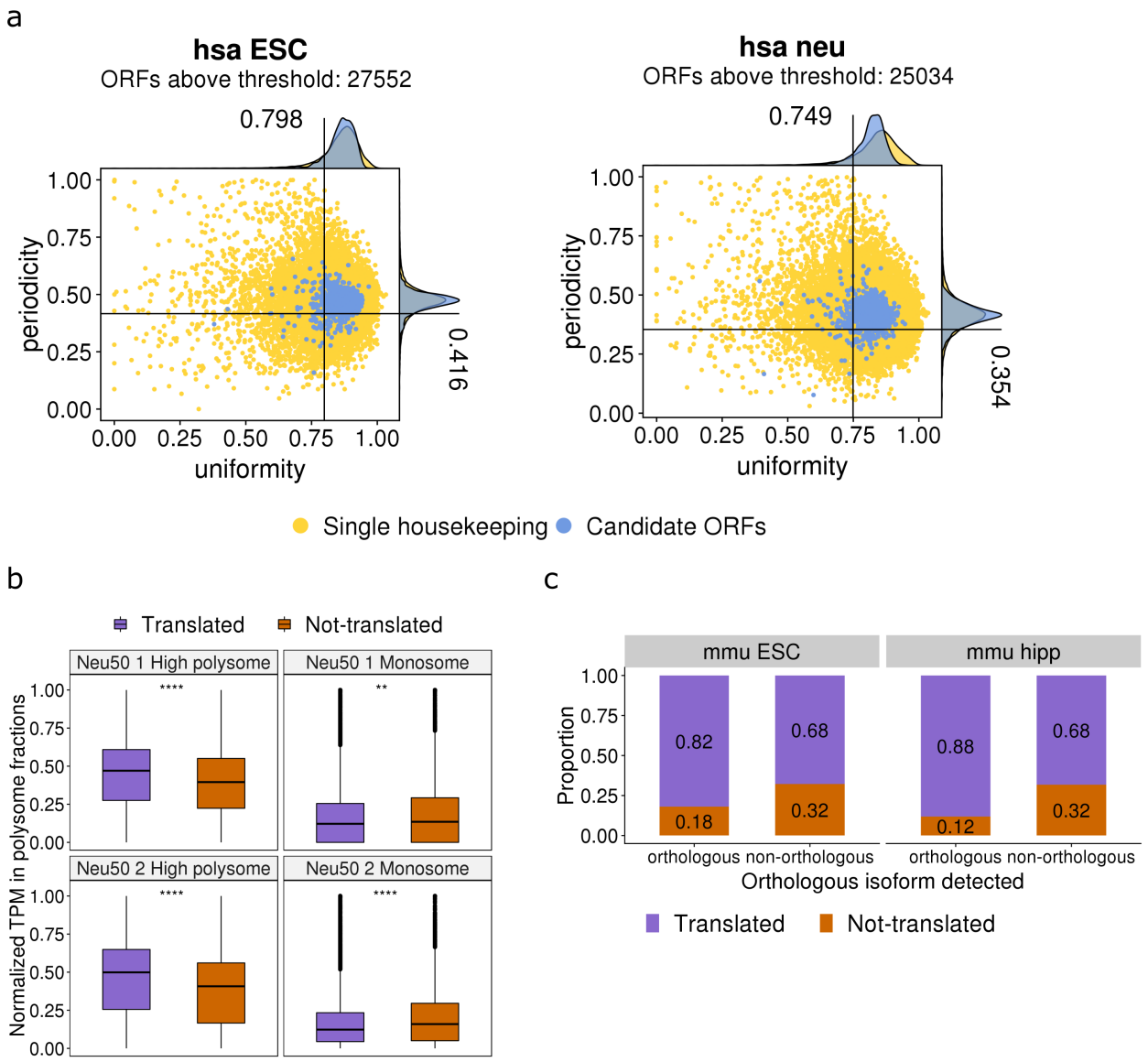


**Supplementary Figure 3. (a)** Uniformity (x axis) versus periodicity (y axis) for the ORFs with with RNA expression TPM > 0.1 and at least 10 Ribo-seq reads assigned. In blue we indicate ORFs from genes defined as housekeeping singletons, and in yellow the rest of ORFs considered. Uniformity is measured as the percentage of maximum entropy and periodicity is measured in the first annotated frame. We show the data for the samples of human ESCs (left panel) and human differentiated neurons (right panel). **(b)** For isoforms predicted to be translated, and for isoforms with enough RNA expression (TPM>0.1) but predicted as not translated, we show the distributions of the relative abundance in monosomes and high polysome fractions (Methods). The plot shows the results for the two replicates for monosome (replicate 1 p-value = 1.21e-03 and replicate 2 p-value = 2.50e-32) and high polysome (replicate 1 p-value = 6.10e-61 and replicate 2 p-value = 6.15e-87) fractions for neuronal cells. **(c)** For the set of ORFs encoding a human-mouse orthologous protein pair (orthologous) and for those encoding proteins without an orthologous pair in mouse (non-orthologous) we plot the percentage that are predicted to be translated (translated)

and the ones that did not pass the uniformity and periodicity thresholds (not-translated). We show here the results for mouse ESCs (p-value = 5.228e-124 Fisher test) and for mouse hippocampus (p-value = 9.821e-311).

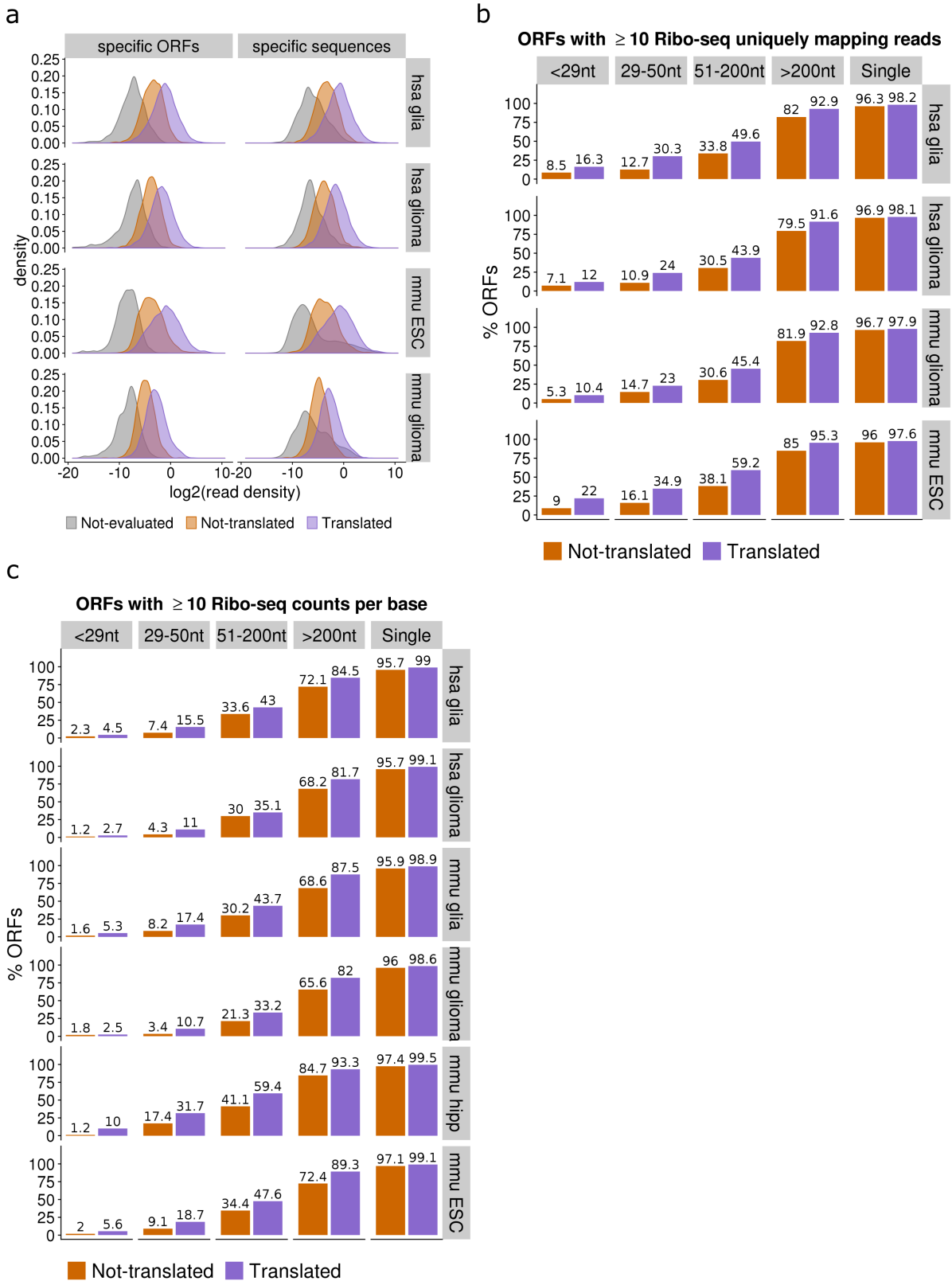


**Supplementary Figure 4. (a)** For the samples of human glia (hsa glia), human glioma (hsa glioma), mouse Embrionic Stem Cells (mmu ESC) and mouse glioma (mmu glioma), we show the density of Ribo-seq reads per nucleotide over the isoform-specific regions, measured as the uniquely mapping read-count over region length in $\log_2$ scale for isoform-specific sequences (right

panels) and the counts per nucleotide based on the estimated P-site positions over region length in $log_2$ scale for isoform-specific ORFs (left panels). Distributions are given for predicted translated isoforms, for isoforms that did not pass the threshold of uniformity and periodicity (not translated), and for the isoforms with low expression (TPM<0.1) (not evaluated). **(b)** For the same samples we show the percentage of regions with at least 10 uniquely mapping Ribo-seq reads in isoform-specific sequences over the total number of isoforms with an isoform-specific sequence defined according to the length of the region. **(c)** We show the percentage of regions with at least 10 Ribo-seq counts in the isoform-specific ORFs considering the estimated P-site position according to the length of the region.

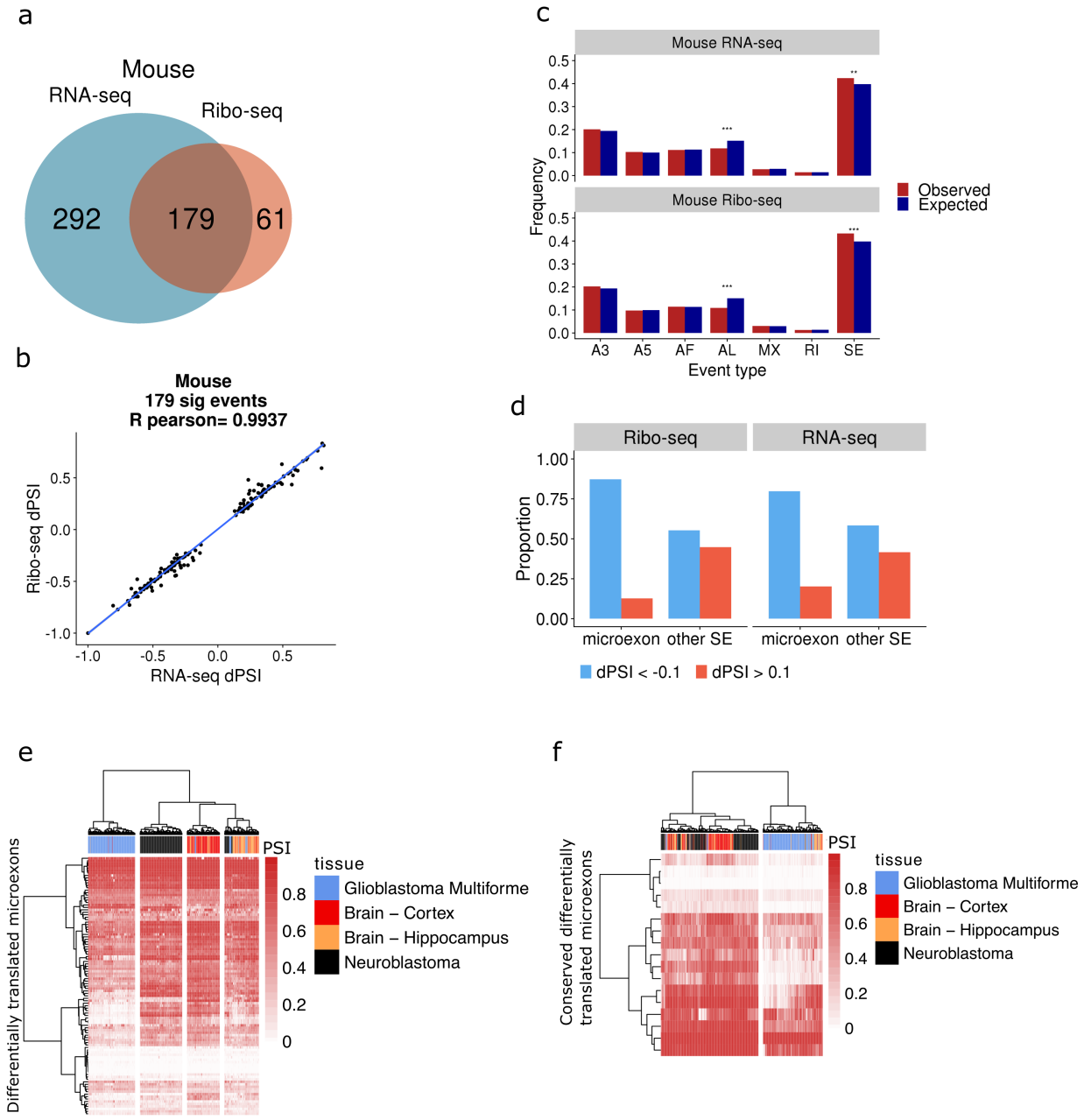


**Supplementary Figure 5. (a)** Overlap of events changing significantly (dPSI > 0.1 and p-value < 0.05) with RNA-seq and with Ribo-seq for mouse. **(b)** Correlation of changes in splicing and translation in events in mouse. **(c) P**roportions of events calculated in RNA space (upper panel) or ribosome space (lower panel). In red we show the proportion of alternative splicing events calculated with SUPPA that overlap coding regions in mouse, whereas in blue we show the events that show a significant change using RNA-seq comparing mouse glia and glioma. Even types are: alternative 3'ss (A3) and 5'ss (A5), alternative first (AF) and last (AL) exon, mutually exclusive (MX) exon, retained introns (RI) and skipping exon (SE). There is significant enrichment of SE events for RNA (Fisher's test p-value = 3.22e-03) and Ribo-seq (p-value = 3.04e-04); and significant depletion of AL events for RNA (2.17e-13) and Ribo-seq (2.86e-18). **(d)** Proportions of

regulated microexons in RNA and Ribosome space for the comparison of glia and glioma samples in mouse. **(e)** Patterns of inclusion of differentially translated microexons in normal brain and hippocampus samples from GTEX, gliblastoma multiforme from TCGA and neuroblastoma from TARGET. The heatmap shows the Percent Spliced In (PSI) values for each sample. **(f)** Patterns of inclusion of conserved differentially translated microexons in normal brain and hippocampus samples from GTEX, gliblastoma multiforme (GBM) from TCGA and neuroblastoma (NB) from TARGET. The heatmap shows the Percent Spliced In (PSI) values for each sample.